



Holographic polymer nanocomposites with simultaneously boosted diffraction efficiency and upconversion photoluminescence

Xiaomei Zhang^a, Weijing Yao^b, Xingping Zhou^a, Wei Wu^{b,*}, Qingkun Liu^c, Haiyan Peng^{a,**}, Jintao Zhu^a, Ivan I. Smalyukh^{d,e}, Xiaolin Xie^a

^a Key Lab for Material Chemistry of Energy Conversion and Storage, Ministry of Education, School of Chemistry and Chemical Engineering, and National Anti-Counterfeit Engineering Research Center, Huazhong University of Science and Technology (HUST), Wuhan, 430074, China

^b Lab of Printable Functional Nanomaterials and Printed Electronics, School of Printing and Packaging, Wuhan University, Wuhan, 430072, China

^c Department of Physics, Cornell University, Ithaca, NY, 14850, United States

^d Department of Physics, Materials Science and Engineering Program, Materials Science and Engineering Center, University of Colorado at Boulder, Boulder, CO, 80309, United States

^e Renewable and Sustainable Energy Institute, National Renewable Energy Laboratory and University of Colorado at Boulder, Boulder, CO, 80309, United States

ARTICLE INFO

Keywords:

Functional composites
Nano composites
Polymer-matrix composites
Interface

ABSTRACT

Holographic polymer nanocomposites have drawn considerable attention due to their unique capability of reconstructing colored three-dimensional (3D) images identifiable to the naked-eye. Yet, it still remains challenging to add more and orthogonal (*i.e.*, data access without crosstalk) optical functions to current holographic polymer nanocomposites. Herein, we design and demonstrate a holographic polymer nanocomposite with robust optical diffraction and upconversion photoluminescence. This paradigm is enabled by controlling the spatial location of upconversion nanorods (UCNRs) in the constructive (polymer-rich) regions during holographic recording, while utilizing the phase separating liquid crystal (LC) in the destructive regions to boost the refractive index difference between the constructive and destructive regions. One identical holographic image is reconstructed and readily visible to the naked-eye under ambient light, whereas four different covert luminescence states (*i.e.*, none, blue, yellowish green and red emissions, respectively) can only be distinguishable upon the 980 nm laser illumination. The double-verifiable and crosstalk-free optical features pave a way to design new tags with orthogonal optical functions for anti-counterfeiting and security applications.

1. Introduction

Polymer nanocomposites with advanced functions have drawn particular attention [1–6]. Holographic polymer nanocomposites are one advanced optical composites that hold the unique capability of reconstructing naked-eye recognizable colored three-dimensional (3D) images, and thus show a great potential to be applied in advanced anti-counterfeiting and security applications [7,8].

Typically, holographic polymer nanocomposites are formed *via in-situ* holographic photopolymerization induced phase separation. In detail, the homogeneous mixture of initiator, monomers and nanoparticles (NPs) are exposed to the laser interference pattern. Photopolymerization of monomers occurs within the constructive (high light intensity) regions after the initiator is excited by the coherent laser. Subsequently, the NPs are squeezed into the destructive (low light

intensity) regions because of the unbalanced chemical potential led by the spatially controlled photopolymerization. One basic requirement for reconstructing holographic polymer nanocomposites is enabling a high diffraction efficiency in a short time. To do this, not only a high refractive index difference between the photo-generated polymer and NPs is required, but also a high degree of phase separation between them is demanded [8]. The segregation degree (*SD*) is used to quantify the phase separation, which is exponentially proportional to the gelation time/viscosity ratio, $SD \sim \exp(t_{gel}/\nu)$ [8]. Nevertheless, despite the extensive demonstration of high performance holographic polymer nanocomposites by using the high refractive index TiO₂ [9–11], ZrO₂ [11–13], ZnS [8], hyperbranched polymer NPs [14,15], CdSe quantum dots [16], and other NPs [17], it still remains challenging to add more and orthogonal (*i.e.*, data access without crosstalk) optical functions to current holographic polymer nanocomposites. Holographic polymer

* Corresponding author.

** Corresponding author.

E-mail addresses: weiwu@whu.edu.cn (W. Wu), hypeng@hust.edu.cn (H. Peng).

nanocomposites with two and more orthogonal optical functions are indispensable for all optical processing devices since the information security is envisioned to be greatly improved.

Since the image and color generated by the holographic polymer nanocomposites are basically structural, loading phosphors is expected to be an effective way to add the orthogonal optical functions to current holographic polymer nanocomposites. Toward this end, Goldenberg and Tomita have fabricated luminescent holographic polymer nanocomposites that are ultraviolet (UV)-sensitive by incorporating LaPO_4 : Ce^{3+} , Tb^{3+} nanoparticles [18] or CdSe quantum dots [16]. The former shows a high diffraction efficiency of 80% while the latter shows a large diffraction efficiency up to 100%. By contrast, here we fabricate luminescent holographic polymer nanocomposites with a diffraction efficiency of $\sim 92\%$ by incorporating near-infrared (NIR) light sensitive upconversion nanocrystals (UCNCs) since the NIR light is less harmful and background-free. Particularly, the lanthanide doped UCNCs represent several distinct advantages. With the step-wise multiphoton absorption upon exposure to the NIR light, UCNCs are able to generate nonlinear anti-Stokes emissions in the UV or visible wavelength regime [19]. More importantly, UCNCs represent distinct characteristics such as large anti-Stokes shift, sharp emission bands, controllable emission wavelength, long photoluminescence lifetime, tunable crystal morphologies and phases [20,21]. In addition, UCNCs with the same morphology and phase but distinctive emission colors are readily achieved [22], which opens the possibility to encode holographic polymer nanocomposites with distinct emission colors. To the best of our knowledge, despite the amazing progress on the design, synthesis and application of UCNCs, the assembly of UCNCs into mesoscale ordered structures using holography is rarely explored. A formidable challenge exists that hinders efforts to simultaneously improve the holographic performance (requiring a high refractive index contrast and large phase separation) and upconversion luminescence (requiring a high UCNC loading). The hurdle is that a high NP loading usually gives rise to deteriorated phase separation, increased light scattering and eventually a depressed diffraction efficiency [23]. Herein, to simultaneously enable the robust upconversion luminescence and bright structural colors in one holographic polymer nanocomposite, we design to spatially place the UCNCs in the constructive (polymer-rich) regions, where the UCNCs and polymer hold a similar refractive index to avoid significant light scattering. At the same time, we employ a phase separating liquid crystal (LC) with a high refractive index to boost the refractive index contrast between the constructive and destructive regions (Fig. 1). During holographic recording, large size UCNCs with anisotropic shape (diameter: ~ 19 nm, length: ~ 100 nm), *i.e.*, upconversion nanorods (UCNRs), are employed to slow down their diffusion during holographic recording so that they are primarily fixed by the growing polymer. In contrast, the small LC molecules diffuse fast to offer a high degree of phase separation with the polymer and UCNRs.

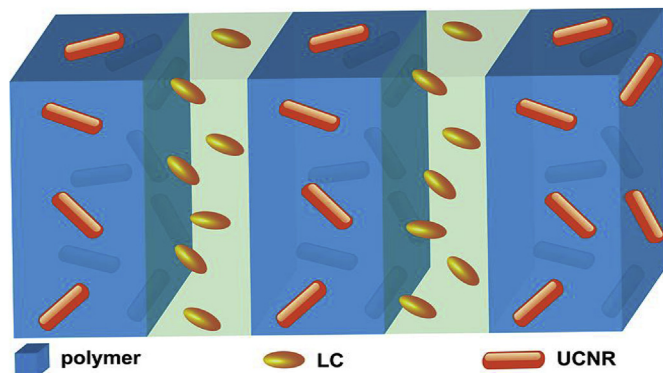


Fig. 1. Scheme illustration of the holographic polymer/LC/UCNR nanocomposites. LC droplets are expected to form in these nanocomposites.

The LC is considered here also because it is able to provide a unique electro-optic response capability [24–26], which is expected to offer more functionalities to the designed polymer nanocomposites. To further boost the degree of phase separation, we increase the miscibility of UCNRs with the polymer matrix while decreasing their miscibility with the LC by dialing the polymer components and LC. Interestingly, both a diffraction efficiency and a strong upconversion emission are simultaneously realized in a single holographic polymer/LC/UCNR nanocomposite. Furthermore, the emission color is dialed to be none, blue, yellowish green and red, respectively, without affecting the diffraction efficiencies.

2. Material fabrication

2.1. Materials

All chemicals were used directly as purchased. No further purification was employed unless this is specially noted. Deionized water was prepared in the lab. $\text{YCl}_3 \cdot 6\text{H}_2\text{O}$ (purity: 99.9%), $\text{YbCl}_3 \cdot 6\text{H}_2\text{O}$ (purity: 99.9%), $\text{ErCl}_3 \cdot 6\text{H}_2\text{O}$ (purity: 99.9%), $\text{TmCl}_3 \cdot 6\text{H}_2\text{O}$ (purity: 99.99%), $\text{GdCl}_3 \cdot x\text{H}_2\text{O}$ (purity: 99.99%), oleic acid (purity: 90%), *N*-phenylglycine (NPG, purity: 99%) and 3,3'-carbonylbis(7-diethylaminocoumarin) (KCD, purity: 99%) were purchased from Sigma-Aldrich. NH_4F (purity: 99.99%) was purchased from Aladdin. Ethyl alcohol (purity: 99.7%), NaOH (purity: 96%) and cyclohexane (purity: 99.7%) were received from Sinopharm Chemical Reagent Co., Ltd., China. *N,N*-Dimethylacrylamide (DMAA, purity: 99%) was purchased from J&K Scientific. The hyperbranched acrylate monomer 6361-100 was donated as a gift by Eternal Chemical Co., Ltd., China. The LC mixture P0616A (refractive indices $n_{o(589 \text{ nm}, 20^\circ\text{C})} = 1.52$, $n_{e(589 \text{ nm}, 20^\circ\text{C})} = 1.72$, nematic-isotropic transition temperature $T_{\text{NI}} = 58^\circ\text{C}$) was obtained from Shijiazhuang Chengzhi Yonghua Display Material Co., Ltd., China.

2.2. Preparation of UCNRs

UCNRs were synthesized according to the Liu's method [27]. In a typical procedure, 1.2 g NaOH was dissolved in 6 mL deionized water, and then mixed with 20 mL ethyl alcohol and 20 mL oleic acid. Subsequently, 8 mL LnCl_3 (0.2 M, Ln = Y, Yb, Er, Tm, Gd) and 4 mL NH_4F (2 M) in water were added dropwise into the former solution under stirring. The resulting solution was transferred into a 100 mL Teflon-lined autoclave and then kept heating at 200°C for 2 h. Following, the autoclave was cooled down to room temperature. The product was isolated *via* centrifugation at a speed of 11,000 rpm (rotor radius: 6 cm) for 8 min. The produced UCNRs were washed for several times with cyclohexane, ethanol and deionized water, consecutively, and finally freeze dried. The chemical compositions of UCNRs were shown in Table S1.

2.3. Fabrication of holographic polymer nanocomposites

The detailed composition of each nanocomposite is shown in Table S2. During the preparation of holographic mixtures, all chemicals were added into a brown-color capped glass vial and then sealed with Parafilm. Subsequently, bulk ultrasonication was employed at room temperature for 40 min to offer homogeneous mixtures. Under red light, a few drops of holographic mixtures were dropped on one side of the glass cell (gap: $10 \mu\text{m}$). With the help of capillary forces, the mixture was encapsulated inside the glass cell under dark conditions. Holographic polymer nanocomposites in the form of periodical gratings were reconstructed as illustrated in Fig. S1a. A 460 nm laser (Genesis MX460-500, Coherent, USA, polarization ratio: linear $> 100:1$, polarization direction: vertical $\pm 5^\circ$) was used as the light source. The glass cell encapsulated with holographic mixtures was put into the laser interference field and exposed for 30 s. The light intensity for each of the

two coherent beams was optimized as 3 mW cm^{-2} when writing all gratings. After holographic recording, the structures were solidified by flood-cure for 500 s with a mercury lamp. Five samples were prepared for each group to provide an average value of the diffraction efficiency with standard deviations. During the holographic image reconstruction, a spatial light modulator (SLM) was used to project the computer-generated image into the interference field as an object beam (Fig. S1b). Images were replicated through the interference of object beam with a reference beam.

3. Characterization

To understand the morphology of UCNRs, transmission electron microscopy (TEM) characterization was performed on Hitachi HT-7700 Compact-Digital TEM. Powder X-ray diffraction (XRD) characterization was employed to study the crystal phase of UCNRs, and the test was performed on the PANalytical X'Pert PRO MPD X-ray diffraction system.

Upconversion emission spectra were recorded using one spectrophotometer (F-4600, Hitachi). The spectrometer was equipped with a 980 nm fiber-coupled laser system (MDL-III-980-2 W, Changchun New Industries Optoelectronics Tech. Co., Ltd, China). The current value of the laser system was set as 1.5.

To characterize the grating morphology, scanning electron microscopy (SEM, Nova NanoSEM 450, FEI) was performed. The glass cells were opened and then samples were cut into small pieces. These small pieces were then immersed in *n*-hexane for 36 h to fully remove the LC. Subsequently, the samples were dried under ambient conditions and coated with a thin layer of platinum, which were followed by the SEM characterization.

An LC display parameter tester (LCT-5016C, North LC Engineering Research and Development Centre, China) and a 633 nm He-Ne laser (HNL 050 L, Thorlabs, USA) were utilized to nondestructively characterize the diffraction efficiency of reconstructed holographic gratings. P-polarized 633 nm light was used unless specially noted. When the 633 nm light irradiated the holographic gratings, diffraction, transmission, reflection and scattering were generated, respectively. The diffraction intensity (I_d), transmission intensity (I_t) and reflection intensity (I_r) at the Bragg angle (θ_B) were easily measured (Fig. S2). Thus, the diffraction efficiency (η) can be calculated as follows,

$$\eta = \frac{I_d}{I_d + I_t} \quad (1)$$

and the scattering light intensity (I_s) can be given as,

$$I_s = I - I_d - I_t - I_r \quad (2)$$

where, I stands for the incident intensity of the 633 nm laser.

4. Results and discussion

4.1. Characterization of UCNRs

Lanthanide-doped NaYF_4 was employed as the UCNC considering its capability of providing a high upconversion efficiency and a similar refractive index (1.46–1.49) to that of polymer matrix (1.47) [19,28]. Three kinds of lanthanide-doped UCNRs (e.g., UCNR-1, UCNR-2 and UCNR-3) with similar sizes but distinct photoluminescence colors were synthesized through the hydrothermal method [27]. Since the content of Gd^{3+} could show a dominant influence on the UCNR dimension during synthesis [27], we fix the Gd^{3+} content at 60 mol % while allowing other lanthanide ions (e.g., Yb^{3+} , Er^{3+} and Tm^{3+}) to change. Therefore, the UCNRs' diameter is controlled to be $19 \pm 4 \text{ nm}$, and their length slightly varies from 89 ± 11 to $116 \pm 23 \text{ nm}$ (Fig. 2).

The XRD patterns confirm that all as-synthesized UCNRs are in hexagonal phase, in good accordance with the JCPDS standard card (file number 16-0334, Fig. 3a). Because of the varied content of Yb^{3+} , Er^{3+} and Tm^{3+} , yellowish green, blue and red photoluminescence

colors are afforded for the UCNR-1, UCNR-2 and UCNR-3, respectively (Fig. 3b and Fig. S3) [27,29], without affecting the crystal size and crystal phase. The main emission peaks locating at 475, 543 and 654 nm are contributed to the optical transitions of Tm^{3+} : $^1\text{G}_4 \rightarrow ^3\text{H}_6$, Er^{3+} : $^2\text{S}_{3/2} \rightarrow ^4\text{I}_{15/2}$, and Er^{3+} : $^4\text{F}_{9/2} \rightarrow ^4\text{I}_{15/2}$, respectively (Table S3) [19,29].

4.2. Design and formulation of holographic polymer nanocomposites

The as-synthesized UCNRs can be well-dispersed in DMAA but immiscible with the LC P0616A (Figs. S4 and S5). Since the solubility parameter is 17.3, 20.3 and $20.5 \text{ J}^{1/2} \text{ cm}^{-3/2}$ for oleic acid, DMAA and P0616A [30], respectively, the good dispersity of oleic acid capped UCNRs in DMAA is expected to be led by the Lewis acid-base interaction.

Holographic polymer/LC/UCNR nanocomposites are formulated as follows. The monomers (e.g., DMAA and 6361-100), LC (e.g., P0616A) and UCNR were mixed homogeneously upon bulk ultrasonication at room temperature. The monomer DMAA was employed to tune the miscibility of the polymer matrix with the oleic acid capped UCNRs. Meanwhile, the hyperbranched monomer 6361-100 provided a high crosslinking density after reaction but a low viscosity for facilitating the monomer and LC diffusion during holography [23]. The photoinitiator comprised of KCD and NPG was used to mediate the holographic photopolymerization, which was selected in our design because of its attractive capability of exerting spatiotemporal control over the photopolymerization kinetics and gelation [7]. Since we hypothesized that the designed UCNRs would be trapped by the growing polymer network and primarily located in the polymer-rich regions, we fixed the LC content at an optimized value of 33 wt% [7,23,24] while varying the monomer-UCNR mass ratio during holography. As a proof of concept, the composites containing the UCNR-1 were initially investigated in details.

We observed a high loading concentration of UCNRs up to 15 wt% in the polymer nanocomposites without significantly affecting the polymerization kinetics, making it possible to multiplex both the optical holography and upconversion luminescence spontaneously. As observed in other mixtures with NPs [8,23], the mixture's viscosity continues to increase exponentially from 6.2 to 23.1 mPa s with an augmentation of the UCNR-1 content from zero to 7.5 vol% (Fig. 4a). According to previous reports [8,31], the density of the synthesized UCNR-1 is calculated to be 4.2 g cm^{-3} . In this case, the volume fraction (f) is estimated as follows:

$$f = \frac{V_i}{\sum V_i} = \frac{\frac{m_i}{\rho_i}}{\sum \frac{m_i}{\rho_i}} \quad (3)$$

where, V_i , m_i and ρ_i are the volume, mass and density of each component in the holographic mixtures, respectively. The relationship between the viscosity (ν) and volume fraction (f) of UCNR-1 can be described as follows:

$$\nu = \nu_0(1 + B(\exp(A \cdot f) - 1)) \quad (4)$$

where ν_0 is the initial viscosity without UCNRs, A represents a constant related to the holographic mixtures, and B is the pre-exponential factor. The value of ν_0 , A and B are calculated to be 6.29, 0.31 and 0.28, respectively. Such viscosity increase usually gives rise to slower molecular diffusion and decreased polymerization rate [8,23]. In contrast, no significant change on the polymerization rate and double bond conversion is observed in the present case (Fig. 4b). Presumably, the UCNRs with a large size provide more free volume for facilitating the monomer diffusion and collision with the active free radicals. The unchanged photoreaction kinetics is envisioned to offer similar photo-rheology behavior, as demonstrated by the insignificantly varied gelation time of $\sim 50 \text{ s}$, when increasing the UCNR-1 loading up to 15 wt% (Fig. 4c). However, the gelation time is significantly decreased down to

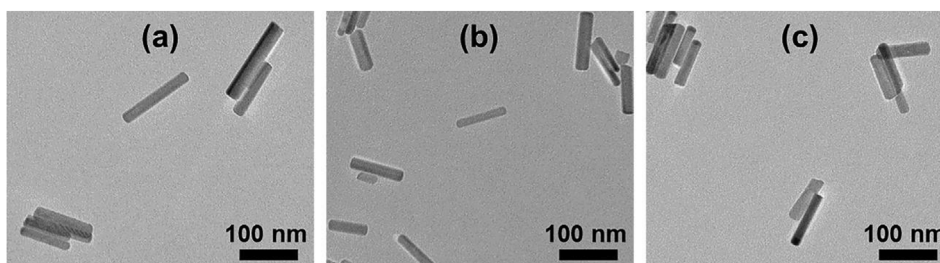


Fig. 2. TEM images of (a) UCNR-1, (b) UCNR-2 and (c) UCNR-3. Their diameter is 19 ± 4 nm and their lengths are 116 ± 23 , 89 ± 11 and 90 ± 16 nm, respectively, showing similar dimensions for these UCNRs.

~30 s when further raising the UCNR-1 loading, because the large amount of rigid inorganic UCNRs give rise to a high storage modulus at the gel point (inset in Fig. 4c and Fig. S6).

4.3. Holographic patterning

Holographic polymer nanocomposite films are readily patterned with the primary location of UCNRs in the constructive (polymer-rich) regions. After injecting the homogeneous monomer/LC/UCNR mixture into glass cells with a controlled gap (10 μm), unslanted transmission gratings with pre-designed pitches (750 nm) are readily fabricated using a two-beam interference technique. During the holographic recording, the photoinitiator absorbs the light and triggers the radical polymerization in the bright regions. Following this, monomers diffuse from the dark regions into the bright regions to participate in the polymerization while the phase-separating LC molecules are squeezed into the dark regions (Fig. S7). For the large size UCNRs, they are expected to be trapped within the constructive regions by the growing polymer network due to the slow diffusion. At the same time, their phase separation with the emerging LC droplets is boosted due to their poor miscibility with the LC. With the optimized laser intensity of 3 mW cm^{-2} for each coherent beam at the wavelength of 460 nm, uniform holographic gratings were obtained under the two-beam interference field. Clearly, the UCNRs are primarily fixed by the *in-situ* generated polymer as pre-designed (Fig. 5). Although small amounts of UCNR-1 leave in the LC-rich region, they do not display a significant influence on the degree of phase separation and refractive index contrast between the constructive and destructive regions. The main location of UCNR-1 in the polymer-rich regions is further confirmed by the detected mass ratio of UCNR-1 to polymer before and after LC removal (*i.e.*, 0.24 and 0.22, respectively), which is close to the pre-designed value 0.28 (Figs. S8 and S9).

4.4. Simultaneously boosted diffraction efficiency and photoluminescence in holographic polymer nanocomposites

Remarkably, a high diffraction efficiency of the holographic polymer/LC/UCNR nanocomposites has been preserved with a high loading of UCNRs because of the completed phase separation and well-formed grating structures with alternating LC-rich (high refractive index) regions and polymer/UCNR-rich (low refractive index) regions. The diffraction efficiency is defined as the ratio of the diffracted light intensity to the sum of diffracted and transmitted light intensities at the Bragg angle. These gratings are in the Bragg regime (*i.e.*, volume gratings) with a quality factor (Q) of 34.2 [32], and they show good symmetry in the angle selective diffraction curve after postcure treatment (Fig. S10). The incident angle dependent diffraction efficiency is fitted with an expression based on the Kogelnik's coupled wave theory [33,34], which gives rise to a refractive index modulation (Δn) of 0.034 for the 10 μm thick composite. When probed at the Bragg angle, the diffraction efficiency (η) can be described as [34]:

$$\eta = \sin^2 \left(\frac{\pi \Delta n d}{\lambda_{\text{probe}} \cos \theta_B} \right) \quad (5)$$

From which, we note that a slight overmodulation is given in our holographic polymer nanocomposites. A maximum diffraction efficiency can be achieved when the Δn equals 0.029 for the 10 μm thick composite (Fig. S11). Moreover, due to the large birefringence of the LC and the preferential orientation of LC molecules along the grating vector, predominant p-polarized diffraction is observed for these holographic polymer/LC/UCNR nanocomposites.

Interestingly, a high diffraction efficiency with a relatively small light scattering loss is achieved in the holographic polymer/LC/UCNR nanocomposites when the UCNR-1 loading is increased to 15 wt% (Fig. S12), which is consistent with the brighter patterns of diffraction than that of transmission (Fig. S13). The probed intensities of reflection, transmission and diffraction can be detected directly. Then, the light

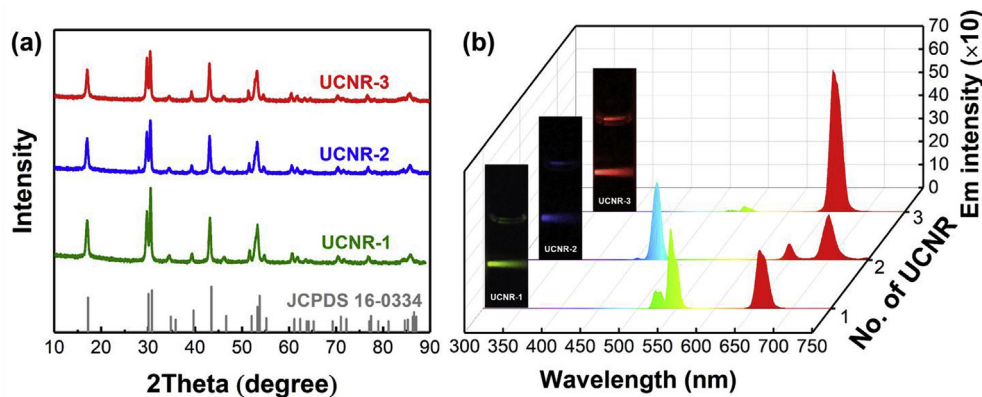


Fig. 3. (a) XRD patterns of UCNRs. (b) Photoluminescence spectra of UCNRs. Each emission (Em) spectrum was measured after dispersing 9 mg UCNRs into 3 g DMAA. The insets are the photoluminescence images of UCNRs in DMAA obtained upon 980 nm laser irradiation.

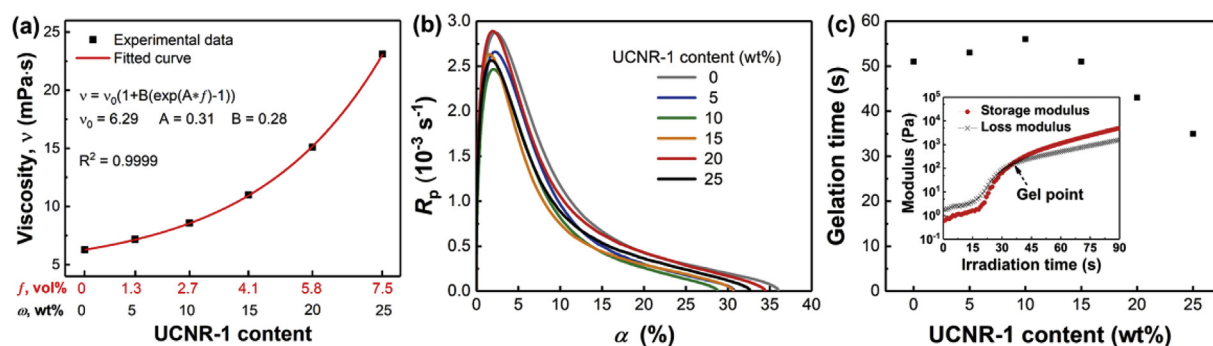


Fig. 4. (a) UCNR content dependent viscosity of the monomer/LC/UCNR mixtures. (b) Rate of polymerization (R_p) versus double-bond conversion (α) of the monomer/LC/UCNR mixtures with varied UCNR content. (c) Gelation time of monomer/LC/UCNR mixtures versus the UCNR-1 loading during photopolymerization. Inset: typical moduli change versus the irradiation time, where the crossover of storage and loss moduli is regarded as the gel point.

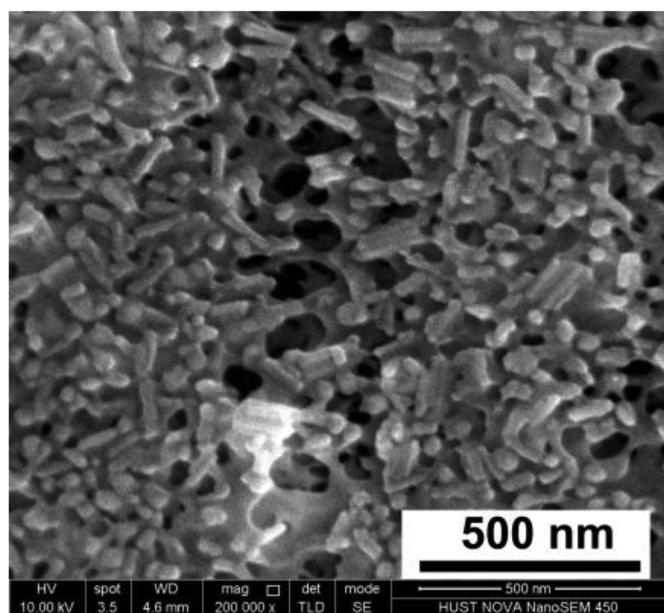


Fig. 5. SEM image of the holographic polymer/LC/UCNR nanocomposite with 15 wt% of UCNR-1 after LC removal. The oval dark holes indicate the original LC droplets (major axis: 75.2 ± 34.0 nm, minor axis: 43.4 ± 18.5 nm). The UCNRs were trapped by the cross-linked polymer.

scattering intensity is calculated by subtracting these three intensities from the incident intensity of the laser source. The diffraction efficiency is found to be $92 \pm 2\%$ even with 15 wt% of UCNR-1 when probed by a non-destructive 633 nm laser (Fig. 6a). Further increasing the UCNR-1 content to 25 wt% gives rise to a decrease of diffraction efficiency to $78 \pm 1\%$. This clear diffraction efficiency drop is primarily caused by the largely increased light scattering and decreased diffraction (Fig. 6b). Yet, only a slight decrease of the driving voltages is observed as the UCNR loading is varied (Fig. S14).

A strong upconversion emission has been demonstrated simultaneously in these holographic polymer nanocomposites with a high diffraction efficiency at a high loading concentration of UCNRs. Clearly, the upconversion emission intensity linearly grows up with an augmentation of the UCNR content once exceeding the threshold of 4 wt% (Fig. 6c and 6d). The accumulated emission intensity within the wavelength range of 510–570 nm increases faster than that within the wavelength range of 640–690 nm when increasing the UCNR-1 content, providing strongly expressed green emission. The synergistically enhanced upconversion emission and diffraction with these UCNRs demonstrate the successful design of holographic polymer/LC/UCNR nanocomposites with orthogonal optical functions.

To further explore the effects of UCNC size and shape on the holographic polymer nanocomposites, other three kinds of lanthanide-doped NaYF_4 UCNCs with different sizes and shapes were synthesized (Fig. S15 and Table S4) and employed to fabricate holographic polymer nanocomposites. The relative content of the LC and UCNRs is adjusted to be 33 wt% and 15 wt%, respectively. Interestingly, the diffraction efficiency doesn't change significantly when increasing the length-diameter ratio from 1.7 ± 0.3 to 6.2 ± 0.6 . However, when further increasing the length-diameter ratio to 12.6 ± 1.4 , the diffraction efficiency dramatically drops to $56 \pm 13\%$ (Fig. S16), due to the poor phase separation structure (Fig. S17).

In addition, we have investigated the influence of grating spacing on the diffraction efficiencies of holographic polymer nanocomposites. The diffraction efficiencies are found to be $95 \pm 3\%$ and $92 \pm 2\%$ when the grating spacing is 500 and 750 nm, respectively (Fig. S18). However, the diffraction efficiency drops down to $42 \pm 5\%$ when the grating spacing increases to 1000 nm. Clearly, with the increase of grating spacing, it becomes more difficult for the UCNRs to diffuse from the dark regions to the bright regions, resulting in the less pronounced phase separation and reduced diffraction efficiency.

4.5. Image storage in holographic polymer nanocomposites

One identical holographic image to the public but four covert photoluminescence states are encoded in the holographic polymer/LC/UCNR nanocomposites because of the simultaneously boosted diffraction efficiencies and upconversion emissions. Holographic image recording was exerted with the assistance of a spatial light modulator (SLM). The SLM was capable of projecting the computer-generated image into space as the object beam, where the digital control is easily realized. Images are reconstructed in the holographic polymer/LC/UCNR nanocomposites when the object beam interferes with the reference beam. After image recording, colorful holographic images are clearly visible to the naked-eye under ambient light (Fig. S18). The color of these transmission-type holographic images is structural and dependent on the viewing angle [33]. Because of the unique electro-optic response capability of LC molecules, the colored images reconstructed in our holographic polymer nanocomposites can be reversibly switched by an applied electric field (Fig. 7 and Appendix B). On the contrary, four different hidden states (e.g., none, yellowish green, blue and red emissions, respectively) can only be identified under the excitation by a 980 nm laser (Fig. 8). As well-recognized, the widely spread fake trademarks associated with goods (e.g., food and medicine) have severely threatened the public health and economy [35]. By taking advantage of the distinctive invisibility of NIR light to the naked-eye [36–38], the double-check and background-free features in our holographic polymer/LC/UCNR nanocomposites open up new opportunities to design advanced anti-forgery tags through a simple one-step method. Moreover, the presented approach with UCNRs

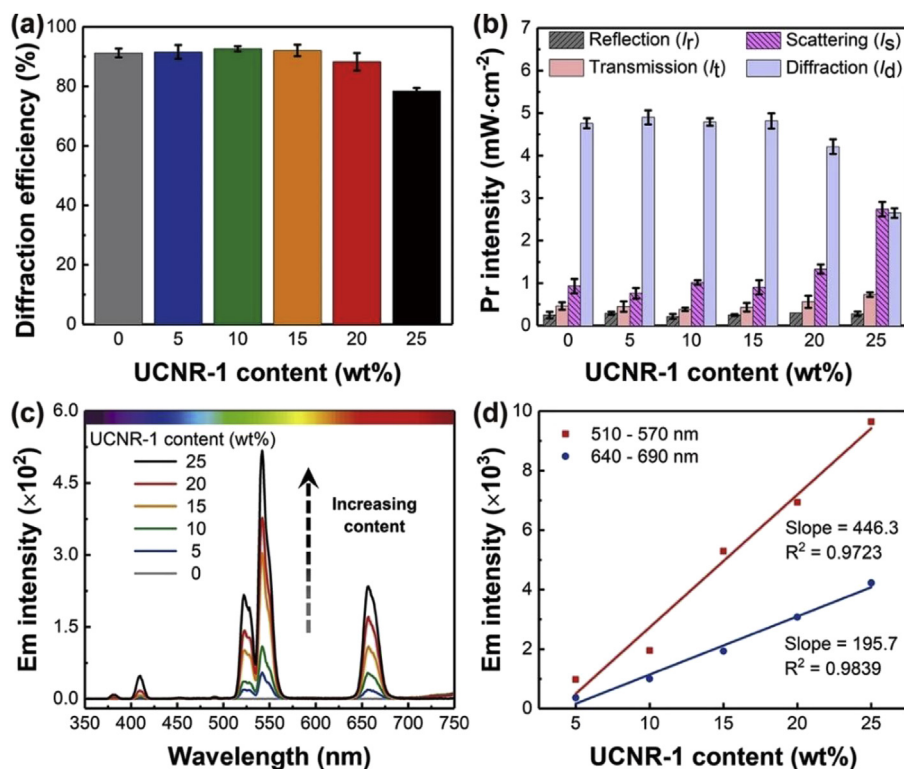


Fig. 6. (a) Diffraction efficiency as a function of the UCNR-1 content. (b) Probed (Pr) intensities of reflection, transmission, scattering and diffraction at the Bragg angle, as a function of the UCNR-1 content. (c) Emission (Em) spectra of the holographic polymer/LC/UCNR nanocomposites with varied UCNR-1 content, when excited by a 2 W 980 nm laser. (d) Integrated emission intensity at the green (510–570 nm) and red (640–690 nm) emission regions as a function of UCNR-1 content. (For interpretation of the references to color in this figure legend, the reader is referred to the Web version of this article.)

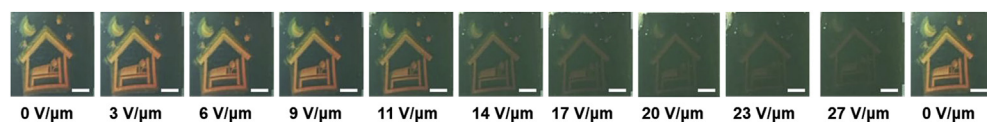


Fig. 7. Holographic image changes in response to applying a continuous square wave voltage. The voltage was AC voltage at a frequency of 1 kHz. 15 wt% UCNR-1 was added in the polymer nanocomposites. All scale bars are 3 mm.

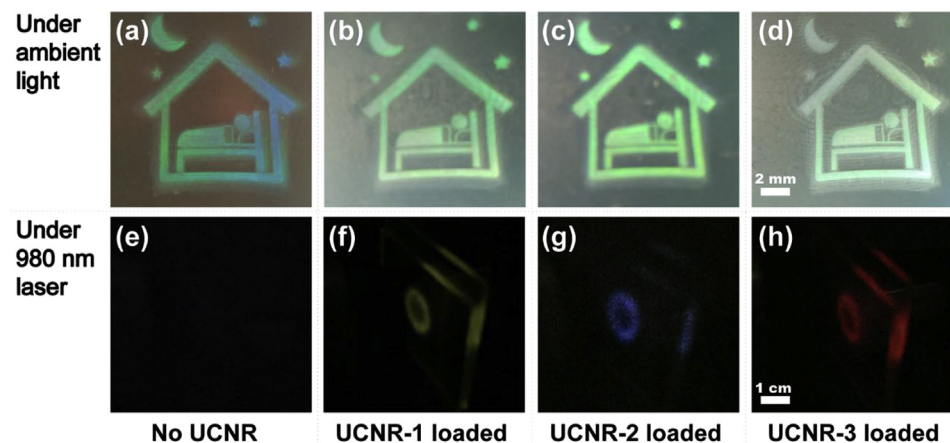


Fig. 8. (a–d) Viewing angle dependent holographic images under ambient light and (e–h) viewing angle independent upconversion emissions under 980 nm laser for the holographic polymer composites. (a, e) no UCNR, (b, f) 15 wt% UCNR-1, (c, g) 15 wt% UCNR-2, (d, h) 15 wt% UCNR-3. The scale bars are 2 mm in a–d, and 1 cm in e–h.

embedded within polymer regions could be also extended to counterparts with the NPs localizing within LC regions and potentially even exhibiting various types of crystalline and biaxial LC organizations [28,39]. This may open a new reach platform for realizing materials with pre-designed optical properties.

5. Conclusions

Synergistically boosted diffraction efficiencies and upconversion emissions were realized in a single holographic polymer/LC/UCNR nanocomposite. This was enabled by controlling the spatial localization of the UCNR during holography. The UCNR was fixed in the polymer-

rich regions that hold a similar refractive index, while the LC with a much higher refractive index was squeezed out. Interestingly, the loading of UCNR could reach 15 wt% without affecting the diffraction efficiency, which gave rise to a high-intensity upconversion emission. In our holographic polymer/LC/UCNR nanocomposites, one identical and publicly disclosed holographic image was reconstructed, which exhibited a viewing-angle dependence and electric switchable capability. Moreover, four different covert photoluminescence states were realized in our holographic polymer/LC/UCNR nanocomposites, paving a new way to design tags with orthogonal optical functions for anti-counterfeiting and security applications.

Acknowledgments

This work is financially supported by the NSFC (51773073, 51433002 and 51503045) and the peak boarding program (HUST). We also thank the support from the NSF of Hubei Scientific Committee (2016CFA001) and the Fundamental Research Funds for the Central Universities (2019kfyRCPY089, 2017KFYXJJ165, 2015ZDTD005). The technical assistance from the HUST Analytical & Testing Center and Miss Min Lei at the Core Facilities of Life and Sciences (HUST) is appreciated. I. S. acknowledges support from the U.S. Department of Energy, Office of Basic Energy Sciences, Division of Materials Sciences and Engineering, under Award ER46921, contract DE-SC0010305 with the University of Colorado at Boulder.

Appendix A. Supplementary data

Supplementary data to this article can be found online at <https://doi.org/10.1016/j.compscitech.2019.107705>.

References

- [1] T.-W. Chou, L. Gao, E.T. Thostenson, Z. Zhang, J.-H. Byun, An assessment of the science and technology of carbon nanotube-based fibers and composites, *Compos. Sci. Technol.* 70 (1) (2010) 1–19.
- [2] H. Fan, D. Fang, L. Chen, Z. Dai, W. Yang, Manufacturing and testing of a CFRC sandwich cylinder with kagome cores, *Compos. Sci. Technol.* 69 (15–16) (2009) 2695–2700.
- [3] C.L. Wu, M.Q. Zhang, M.Z. Rong, K. Friedrich, Silica nanoparticles filled polypropylene: Effects of particle surface treatment, matrix ductility and particle species on mechanical performance of the composites, *Compos. Sci. Technol.* 65 (3–4) (2005) 635–645.
- [4] A. Baji, Y.-W. Mai, S.-C. Wong, M. Abtahi, P. Chen, Electrospinning of polymer nanofibers: effects on oriented morphology, structures and tensile properties, *Compos. Sci. Technol.* 70 (5) (2010) 703–718.
- [5] W. Chen, Z. Wang, C. Zhi, W. Zhang, High thermal conductivity and temperature probing of copper nanowire/upconversion nanoparticles/epoxy composite, *Compos. Sci. Technol.* 130 (2016) 63–69.
- [6] L. Fang, T. Fang, X. Liu, Y. Ni, C. Lu, Z. Xu, Precise stimulation of near-infrared light responsive shape-memory polymer composites using upconversion particles with photothermal capability, *Compos. Sci. Technol.* 152 (2017) 190–197.
- [7] H. Peng, S. Bi, M. Ni, X. Xie, Y. Liao, X. Zhou, Z. Xue, J. Zhu, Y. Wei, C.N. Bowman, Y.-W. Mai, Monochromatic visible light “photoinitiator”: Janus-faced initiation and inhibition for storage of colored 3D images, *J. Am. Chem. Soc.* 136 (25) (2014) 8855–8858.
- [8] M. Ni, H. Peng, Y. Liao, Z. Yang, Z. Xue, X. Xie, 3D image storage in photopolymer/ZnS nanocomposites tailored by “photoinitiator”, *Macromolecules* 48 (9) (2015) 2958–2966.
- [9] N. Suzuki, Y. Tomita, T. Kojima, Holographic recording in TiO₂ nanoparticle-dispersed methacrylate photopolymer films, *Appl. Phys. Lett.* 81 (22) (2002) 4121–4123.
- [10] C. Sánchez, M.J. Escuti, C. Van Heesch, C.W.M. Bastiaansen, D.J. Broer, J. Loos, R. Nussbaumer, TiO₂ nanoparticle-photopolymer composites for volume holographic recording, *Adv. Funct. Mater.* 15 (10) (2005) 1623–1629.
- [11] O.V. Sakhno, L.M. Goldenberg, J. Stumpe, T.N. Smirnova, Surface modified ZrO₂ and TiO₂ nanoparticles embedded in organic photopolymers for highly effective and UV-stable volume holograms, *Nanotechnology* 18 (10) (2007) 105704.
- [12] N. Suzuki, Y. Tomita, Highly transparent ZrO₂ nanoparticle-dispersed acrylate photopolymers for volume holographic recording, *Opt. Express* 14 (26) (2006) 12712–12719.
- [13] G. Georg, L.M. Goldenberg, O.V. Sakhno, A. Markus, N. Markus, S. Joachim, Large-scale synthesis of organophilic zirconia nanoparticles and their application in organic-inorganic nanocomposites for efficient volume holography, *Small* 3 (9) (2010) 1626–1632.
- [14] Y. Tomita, K. Furushima, K. Ochi, K. Ishizu, A. Tanaka, M. Ozawa, M. Hidaka, K. Chikama, Organic nanoparticle (hyperbranched polymer)-dispersed photopolymers for volume storage, *Appl. Phys. Lett.* 88 (7) (2006) 071103.
- [15] Y. Tomita, H. Urano, T.-a. Fukamizu, Y. Kametani, N. Nishimura, K. Odoi, Nanoparticle-polymer composite volume holographic gratings dispersed with ultrahigh-refractive-index hyperbranched polymer as organic nanoparticles, *Opt. Lett.* 41 (6) (2016) 1281–1284.
- [16] X. Liu, Y. Tomita, J. Oshima, K. Chikama, K. Matsubara, T. Nakashima, T. Kawai, Holographic assembly of semiconductor CdSe quantum dots in polymer for volume Bragg grating structures with diffraction efficiency near 100%, *Appl. Phys. Lett.* 95 (26) (2009) 261109.
- [17] Y. Tomita, E. Hata, K. Momose, S. Takayama, X. Liu, K. Chikama, J. Klepp, C. Pruner, M. Fally, Photopolymerizable nanocomposite photonic materials and their holographic applications in light and neutron optics, *J. Mod. Opt.* 63 (2016) S1–S31.
- [18] O.V. Sakhno, T.N. Smirnova, L.M. Goldenberg, J. Stumpe, Holographic patterning of luminescent photopolymer nanocomposites, *Mater. Sci. Eng. C* 28 (1) (2008) 28–35.
- [19] B. Zhou, B. Shi, D. Jin, X. Liu, Controlling upconversion nanocrystals for emerging applications, *Nat. Nanotechnol.* 10 (11) (2015) 924–936.
- [20] X. Li, Z. Guo, T. Zhao, Y. Lu, L. Zhou, D. Zhao, F. Zhang, Filtration shell mediated power density independent orthogonal excitations-emissions upconversion luminescence, *Angew. Chem. Int. Ed.* 55 (7) (2016) 2464–2469.
- [21] J.M. Meruga, W.M. Cross, P.S. May, Q. Luu, G.A. Crawford, J.J. Kellar, Security printing of covert quick response codes using upconverting nanoparticle inks, *Nanotechnology* 23 (39) (2012) 395201.
- [22] J. Lee, P.W. Bisso, R.L. Srinivas, J.J. Kim, A.J. Swiston, P.S. Doyle, Universal process-inert encoding architecture for polymer microparticles, *Nat. Mater.* 13 (5) (2014) 524–529.
- [23] M. Ni, G. Chen, H. Sun, H. Peng, Z. Yang, Y. Liao, Y. Ye, Y. Yang, X. Xie, Well-structured holographic polymer dispersed liquid crystals by employing acrylamide and doping ZnS nanoparticles, *Mater. Chem. Front.* 1 (2) (2017) 294–303.
- [24] M. Ni, H. Peng, X. Xie, Structure regulation and performance of holographic polymer dispersed liquid crystals, *Acta Polym. Sin.* 48 (10) (2017) 1557–1573.
- [25] H. Peng, G. Chen, M. Ni, Y. Yan, J. Zhuang, V.A.L. Roy, R.K.Y. Li, X. Xie, Classical photopolymerization kinetics, exceptional gelation, and improved diffraction efficiency and driving voltage in scaffolding morphological H-PDLCs afforded using a photoinitiator, *Polym. Chem.* 6 (48) (2015) 8259–8269.
- [26] T.J. White, L.V. Natarajan, V.P. Tondiglia, P.F. Lloyd, T.J. Bunning, C.A. Guymon, Monomer functionality effects in the formation of thiol-ene holographic polymer dispersed liquid crystals, *Macromolecules* 40 (4) (2007) 1121–1127.
- [27] F. Wang, Y. Han, C.S. Lim, Y.H. Lu, J. Wang, J. Xu, H.Y. Chen, C. Zhang, M.H. Hong, X.G. Liu, Simultaneous phase and size control of upconversion nanocrystals through lanthanide doping, *Nature* 463 (7284) (2010) 1061–1065.
- [28] H. Mundoor, S. Park, B. Senyuk, H.H. Wensink, I.I. Smalyukh, Hybrid molecular-colloidal liquid crystals, *Science* 360 (6390) (2018) 768–771.
- [29] Q. Chen, X. Xie, B. Huang, L. Liang, S. Han, Z. Yi, Y. Wang, Y. Li, D. Fan, L. Huang, X. Liu, Confining excitation energy in Er³⁺-sensitized upconversion nanocrystals through Tm³⁺-mediated transient energy trapping, *Angew. Chem. Int. Ed.* 56 (26) (2017) 7605–7609.
- [30] D.W.v. Krevelen, K.t. Nijenhuis, *Properties of Polymers*, Elsevier Science, Amsterdam, 2009, pp. 290–296.
- [31] Y.L. Dai, H.H. Xiao, J.H. Liu, Q.H. Yuan, P.A. Ma, D.M. Yang, C.X. Li, Z.Y. Cheng, Z.Y. Hou, P.P. Yang, J. Lin, In vivo multimodality imaging and cancer therapy by near-infrared light-triggered *trans*-platinum pro-drug-conjugated upconversion nanoparticles, *J. Am. Chem. Soc.* 135 (50) (2013) 18920–18929.
- [32] T.J. Bunning, L.V. Natarajan, V.P.T., R.L. Sutherland, Holographic polymer-dispersed liquid crystals (H-PDLCs), *Annu. Rev. Mater. Res.* 30 (1) (2000) 83–115.
- [33] H. Peng, D.P. Nair, B.A. Kowalski, W. Xi, T. Gong, C. Wang, M. Cole, N.B. Cramer, X. Xie, R.R. McLeod, C.N. Bowman, High performance graded rainbow holograms via two-stage sequential orthogonal thiol-click chemistry, *Macromolecules* 47 (7) (2014) 2306–2315.
- [34] H. Kogelnik, Coupled wave theory for thick hologram gratings, *Bell Syst. Tech. J.* 48 (9) (1969) 2909–2927.
- [35] R. Arppe, T.J. Sorensen, Physical unclonable functions generated through chemical methods for anti-counterfeiting, *Nat. Rev. Chem.* 1 (4) (2017) 0031.
- [36] X. Liu, Y. Wang, X. Li, Z. Yi, R. Deng, L. Liang, X. Xie, D.T.B. Loong, S. Song, D. Fan, A.H. All, H. Zhang, L. Huang, X. Liu, Binary temporal upconversion codes of Mn²⁺-activated nanoparticles for multilevel anti-counterfeiting, *Nat. Commun.* 8 (1) (2017) 899.
- [37] J. Zhao, D. Jin, E.P. Schartner, Y. Lu, Y. Liu, A.V. Zvyagin, L. Zhang, J.M. Dawes, P. Xi, J.A. Piper, E.M. Goldys, T.M. Monro, Single-nanocrystal sensitivity achieved by enhanced upconversion luminescence, *Nat. Nanotechnol.* 8 (10) (2013) 729–734.
- [38] Y. Lu, J. Zhao, R. Zhang, Y. Liu, D. Liu, E.M. Goldys, X. Yang, P. Xi, A. Sunna, J. Lu, Y. Shi, R.C. Leif, Y. Huo, J. Shen, J.A. Piper, J.P. Robinson, D. Jin, Tunable lifetime multiplexing using luminescent nanocrystals, *Nat. Photonics* 8 (1) (2014) 32–36.
- [39] H. Mundoor, B. Senyuk, I.I. Smalyukh, Triclinic nematic colloidal crystals from competing elastic and electrostatic interactions, *Science* 352 (6281) (2016) 69–73.